RSC Advances

PAPER

View Article Online
View Journal | View Issue

Cite this: *RSC Adv.*, 2026, **16**, 14036

Photocatalytic degradation of ibuprofen on titanium oxide nanoparticles: insights into degradation kinetics, mechanisms, thermodynamics, pathways, and toxicity

Harry Lik Hock Lau,[a] Rusydi R. Sofian,[a] Syahirah Nabilah Aedy Aewandy,[a] Nur Diana Bazilah Awang Idris,[a] Nur Aisyah Abdul Munir,[a] Nur Nabaahah Roslan,[a] Hussein Taha,[b] Muhammad Nur[c] and Anwar Usman *[a]

The photocatalytic degradation of ibuprofen (IBU) in aqueous solution using titanium dioxide nanoparticles (TiO_2 NPs) as a photocatalyst activated by 365 nm UV light irradiation was systematically investigated. The degradation of IBU was monitored by absorption spectroscopy, and the resulting overlapping spectra were deconvoluted to determine the concentrations of residual IBU and its photocatalytic degradation products. Effective immobilization and strong affinity of IBU for the photocatalyst surfaces were evidenced by the maximum adsorption capacity of 126 ± 4 mg g^{-1} on TiO_2 NPs. Liquid chromatography-mass spectrometry and Fourier-transform infrared spectroscopy revealed that the stable photocatalytic degradation products were 1-(4-isobutylphenyl)ethanol, 4-isobutylbenzaldehyde, and 4-isobutyl-1-ethylbenzene, rather than complete mineralization to carbon dioxide and water. The degradation pathways were proposed to involve hydroxyl radical ($OH^{\bullet}$) attack on the carboxylic group of IBU, leading to the formation of short-lived intermediates, followed by decarboxylation, hydroxylation, and demethylation reactions. The photocatalytic degradation was endothermic and spontaneous, accompanied by an increase in disorder. Based on the simplified Langmuir–Hinshelwood model, the observed degradation rate constant was 1.31 ± 0.02 × 10^{-2} min^{-1}, primarily governed by mass transfer from the bulk solution to the photocatalyst surfaces. Toxicity assessments indicated that the photocatalytic degradation products of IBU are less toxic toward *Artemia salina* larvae, suggesting a reduced toxicity risk to microorganisms in the environment.

Received 31st December 2025
Accepted 8th March 2026

DOI: 10.1039/d5ra10114j

rsc.li/rsc-advances

1. Introduction

Pharmaceutically active compounds, including antibiotics, non-steroidal anti-inflammatory drugs (NSAIDs), analgesics, antipyretics, steroidal hormones, antidepressants, stimulants, and β-blockers, are an increasingly prevalent class of emerging contaminants found in the aquatic environments across various countries.[1] Their presence in the environment is mainly attributed to anthropogenic activities, such as human excretion, improper disposal, and illegal sewage discharge, entering water bodies through domestic wastewater, healthcare waste, and effluents from pharmaceutical industries.[2] Even at low concentrations, pharmaceutically active compounds can exert adverse effects on aquatic ecosystems.[3] For example, antibiotics and NSAIDs present in the environment can induce cytotoxicity, biochemical disruption, behavioral alterations, oxidative cellular stress, and genotoxic damage in aquatic organisms, including *Lemna minor* (duckweed), *Aliivibrio fischeri* (bioluminescent bacteria), *Daphnia magna* (water flea), and *Danio rerio* (zebrafish).[4,5] Moreover, the presence of antibiotics and NSAIDs has been associated with the development of antimicrobial resistance genes, which are potentially transferred to higher trophic levels.[6]

One of the NSAIDs frequently detected in aquatic environments is ibuprofen (IBU; 2-(4-isobutylphenyl)propionic acid), which is widely used as an analgesic, antipyretic, and anti-inflammatory agent for the treatment of inflammatory diseases, pain, fever, rheumatoid disorders, dysmenorrhea, and osteoarthritis.[7] Global prescriptions of IBU exceed 20 million administrations annually, and nearly 15% of the administered dose is excreted as the unchanged parent compound. Actual usage is likely much higher due to its widespread availability as an over-the-counter medication. Consequently, IBU concentrations in wastewater effluents range from several nanograms per

[a]*Department of Chemistry, Faculty of Science, Universiti Brunei Darussalam, Jalan Tungku Link, Gadong BE1410, Brunei Darussalam. E-mail: anwar.usman@ubd.edu.bn*
[b]*Environmental and Life Sciences, Faculty of Science, Universiti Brunei Darussalam, Jalan Tungku Link, Gadong BE1410, Brunei Darussalam*
[c]*Center for Plasma Research, Integrated Laboratory, Universitas Diponegoro, Tembalang Campus, Semarang 50275, Indonesia*

liter to a few tens of milligrams per liter.[8] Because conventional sewage treatment plants are generally unable to completely remove pharmaceutical compounds, IBU is frequently detected in surface waters and poses potential risks to human health and aquatic ecosystems.[9,10] Both *in vivo* and *in vitro* studies have revealed that long-term exposure to IBU is associated with elevated oxidative cellular stress, genotoxic and cytotoxic effects, as well as abnormal growth, reproduction suppression, and behavioral alterations in *Dreissena polymorpha* (zebra mussel).[11]

As IBU is non-biodegradable in nature, the development and implementation of effective methods for its removal from wastewater are indispensable. Adsorption has been widely explored for the removal of IBU from wastewater using various adsorbents, such as activated carbon,[12] biochar,[13] chitosan,[14] and silica nanocomposites.[15] Although adsorption can achieve high removal efficiency, secondary pollution arising from the lack of proper post-adsorption treatment of spent adsorbents remains a critical concern.[2] On the other hand, various advanced oxidation processes (AOPs), including UV/H_2O_2 treatment,[16] ozonation,[17] the photo-Fenton process,[18] and photocatalysis,[19–21] have been applied to generate reactive oxygen species to oxidize and degrade IBU.[22] Several studies have reported IBU degradation without definitive evidence, whereas photocatalysis studies clearly revealed the formation of 1-(4-isobutylphenyl)ethanol.[19,21] This observation suggests that the aromatic ring of IBU remains intact and that, unexpectedly, IBU does not undergo complete mineralization under AOP treatments. The heterogeneous photocatalytic degradation processes and pathways of IBU have been scarcely reported, with only a few studies by Miranda *et al.*,[19] Khendra *et al.*,[20] and Jallouli *et al.*[21] In these earlier works, the feasibility and efficiency of photocatalytic degradation of IBU using TiO_2 under UV irradiation were evaluated, and the existence of 1-(4-isobutylphenyl)ethanol along with related transformation products were identified. However, comprehensive studies on the kinetics, mechanisms, and thermodynamics of IBU photocatalytic degradation have not yet been evaluated, most likely due to the significant overlap between the absorption spectra of IBU and those of its photocatalytic degradation products.[23] Moreover, a quantitative comparison of the photocatalytic degradation behavior of IBU with those of other drugs, as well as an evaluation of the toxicity of degradation products of IBU, remains a research gap.

Therefore, the present work aims to investigate the detailed photocatalytic degradation of IBU on anatase titanium dioxide nanoparticles (TiO_2 NPs) activated under UV light irradiation. Since the pioneering experiment investigating electrochemical photolysis of water on a TiO_2 electrode in 1972 by Fujishima and Honda,[24] TiO_2 NPs have been widely utilized as photocatalysts. Their chemical stability, non-toxicity, cost effectiveness, and high photoactivity for generating $O_2^{\bullet-}$ and $OH^{\bullet}$ radicals make TiO_2 NPs activated under UV light irradiation suitable for the photocatalytic degradation of a broad spectrum of organic pollutants, including synthetic dyes, pharmaceuticals, pesticides, phenolic compounds, and endocrine-disrupting chemicals in water matrices. To overcome the limitations associated with UV light irradiation, extensive efforts have been devoted to modifying TiO_2 through metal and non-metal doping, as well as coupling with organic semiconductors. In particular, 6,13-pentacenequinone/TiO_2 organo–inorganic nanocomposite has been reported to exhibit superior photoactivity under solar and visible light irradiation.[25]

In this study, the overlapping absorption spectra were carefully deconvoluted to determine the concentrations of IBU and its photocatalytic degradation products. The effects of various experimental parameters, including the initial IBU concentration, TiO_2 NP dosage, pH of the medium, temperature, and the addition of hydrogen peroxide (H_2O_2), on the photocatalytic degradation of the NSAID were systematically examined. The objectives of this study are to elucidate the degradation kinetics, rate-limiting steps, and thermodynamic parameters by fitting the experimental data to the Langmuir–Hinshelwood (L–H), Weber–Morris (W–M) intraparticle diffusion, Arrhenius, and Eyring models. The photocatalytic degradation pathways of IBU were interpreted based on degradation products identified using liquid chromatography-mass spectrometry (LC-MS) and Fourier-transform infrared (FTIR) spectroscopy. Finally, the antibacterial activity and brine shrimp lethality of the degradation products were evaluated using the standard screening methods to assess their potential environmental risks. Overall, this study provides a comprehensive understanding of the photocatalytic degradation kinetics, mechanisms, thermodynamic parameters, and pathways of IBU. It also addresses existing knowledge gaps regarding its photocatalytic degradation behavior, and evaluates the environmental safety of the resulting degradation products.

2. Experimental

2.1 Chemicals

IBU sodium salt (CAS: 31,12193-4, $C_{13}H_{17}NaO_3$; 228.26 g mol^{-1}), sodium hydroxide (NaOH; CAS: 1310-73-2], hydrochloric acid (HCl; CAS: 7647-01-0), hydrogen peroxide (30% H_2O_2; CAS: 7722-84-1), *para*-benzoquinone (*p*-BQ; CAS: 106-51-4), *tert*-butanol (*t*-BuOH; CAS: 75-65-0), and TiO_2 NPs (CAS: 13463-67-7; average particle size of 100 nm) were all procured from Sigma-Aldrich Co. (St. Louis, MO, USA). They were used as received.

2.2 IBU stock solutions

In this study, fresh IBU solutions at concentrations in the range from 200 mg L^{-1} to 1000 mg L^{-1} were systematically prepared by dissolving the required amount of solid sodium IBU in 250 mL volumetric flasks containing ultrapure water. The flasks were wrapped with aluminium foil and stored in the dark to prevent photolysis by stray light before use. The absorption spectra of the prepared IBU solutions were measured daily in the range of 200–800 nm using a UV-1900 spectrophotometer (Shimadzu, Kyoto, Japan) to monitor the concentration and stability of the IBU solutions before use in each experiment.

2.3 Characterizations of photocatalyst

As received commercial TiO_2 NPs were used as the photocatalyst in all photocatalytic degradation experiments of IBU. The crystalline phase, band gap energy, BET specific surface area, and particle size of the TiO_2 NPs were confirmed based on X-ray diffraction pattern measured using an XRD-7000 (Shimadzu, Japan) with collimated Cu Kα radiation (λ = 0.15418 nm), diffuse reflectance UV-vis spectroscopy monitored on a UV-2600i (Shimadzu, Japan), multipoint nitrogen gas adsorption–desorption measured using a surface area and porosity analyzer ASAP 2460 (Micromeritics Instrument, USA), and dynamic light scattering (DLS) microscopic characterization using a digital correlator DLS (BI 9000, Brookhaven Instruments Corp.) equipped with a diode-pumped laser (532 nm; 10 mW). The XRD pattern confirmed the anatase phase of the TiO_2 NPs. The Tauc plot revealed a band gap energy of 3.2 eV. The average particle size of TiO_2 NPs was 100 nm with a BET specific surface area of 12.791 $m^2\ g^{-1}$. The photocatalyst characterization results are summarized in Fig. S1 and have been described in our previous publications.[26–29]

2.4 Adsorption of ibuprofen on TiO_2 NPs

IBU solutions with various concentrations, ranging from 200 mg L^{-1} to 1000 mg L^{-1}, were prepared. For each experiment, 20 mL of IBU solution was added to a 7.5 cm diameter glass Petri dish containing 10 mg TiO_2 NPs. The mixtures were gently stirred using a magnetic stirrer for 100 minutes in the dark. After centrifugation at 3500 rpm for 10 minutes using a Centrifuge 5427R (Eppendorf, Germany), the separated IBU solutions were collected, and their absorption spectra were recorded in a 1-cm quartz cuvette cell over the range of 200–800 nm using UV-vis absorption spectroscopy.

Based on the absorption spectra of the IBU solutions, the absorbance was plotted as a function of the initial IBU concentration (C_0), from which the molar extinction coefficient of IBU was estimated to be 254.74 $\pm$ 2.79 L mol^{-1} cm^{-1} at 262.5 nm (see Fig. S2), consistent with the range reported by Du *et al.*[30] This value was subsequently used to determine the concentrations of the NSAID before and after the adsorption process using the Beer–Lambert law.

Each adsorption experiment was repeated in duplicate, and the average value was used in further analysis. The adsorption of IBU on the photocatalyst surfaces was quantified by the adsorption capacity (Q_e), calculated as

$$Q_e = (C_0 - C_e) \times V/m \quad (1)$$

where, C_0 and C_e (in mg L^{-1}) denote the IBU concentration before and after adsorption, V (in mL) is the volume of solution and m (in g) is the mass of TiO_2 NPs.

The adsorption capacity of IBU on TiO_2 NPs was measured at various C_0 values, and the resulting isotherm data were fitted using the nonlinear equations of the Dubinin–Radushkevich, Elovich, Freundlich, Jovanović, Langmuir, and Temkin models. The basic theoretical concepts, mechanisms, and assumptions of each model have been reported in the literature.[31–34] However, it is important to emphasize that photocatalysis occurs on the surface of a photocatalyst activated by light irradiation; therefore, the immobilization of IBU is expected to form only a single monolayer before being oxidized by the generated reactive oxygen species, consistent with the Langmuir isotherm model;[29]

$$Q_e = Q_m K_L C_e/(1 + K_L C_e) \quad (2)$$

where, Q_m denotes the maximum adsorption capacity, and K_L is the Langmuir isotherm constant, representing the affinity of IBU onto the surfaces of TiO_2 NPs.

2.5 Photolysis and photocatalysis

Photolytic and photocatalytic degradation of IBU (200 mg L^{-1}) were evaluated by irradiating 20 mL of the solution in a glass Petri dish (7.5 cm in diameter and 5 cm in high) covered with a UV-transparent watch glass, in the absence and presence of 2.5 mg TiO_2 NPs, respectively. The Petri dish was placed inside a light-tight box to prevent exposure to stray light. The solution was gently stirred using a temperature-controlled magnetic stirrer, while the photocatalyst suspension in the solution was irradiated with a 365-nm fluorescent lamp (Vilber Lourmat, 6W, 211 mm; Marne-la-Vallée Cedex, France) positioned 10 cm above the Petri dish. The UV light intensity at the solution was adjusted to 0.28 mW cm^{-2} using a neutral-density filter. The setup has described in our previous studies.[28,29,35] After a specified irradiation time, typically ranging from 0 to 180 minutes, the solution was collected. For photocatalysis, the photocatalyst was then separated by centrifugation. The absorption spectrum of each solution was recorded over the range of 200–800 nm using UV-vis absorption spectroscopy. The concentrations of IBU before and after photolysis or photocatalysis were determined from the absorption spectra and denoted as C_0 and C_t (in mg L^{-1}), respectively.

It should be noted that the use of high IBU concentrations in adsorption, photolytic, and photocatalytic experiments, exceeding those reported in surface water and groundwater (ng–mg L^{-1} range)[8] is primarily for analytical purposes. In particular, with the relatively low molar extinction coefficient of 254.74 L mol^{-1} cm^{-1} such high IBU concentrations are required to obtain quantifiable absorption spectral changes, allowing more accurate determination of IBU concentrations and, consequently, more reliable insights into the degradation mechanisms, kinetics, and rate-limiting steps. In real wastewater matrices, although the presence of inorganic ions and natural organic matters may compete for reactive species and affect photocatalytic degradation efficiency of IBU, the intrinsic kinetic rate constants, rate-limiting steps, degradation pathways, and dominant reactive species are expected to remain unchanged.[36] Therefore, in general, the photocatalytic degradation behavior of IBU can be extrapolated across different concentration scales.

The photocatalytic degradation of IBU was further evaluated at an irradiation time of 100 minutes under various photocatalyst dosages ranging from 2.5 mg to 15 mg, pH levels of the medium in the range of 4–10, adjusted by adding a few drops of 0.1 M HCl or 0.1 M NaOH into the IBU solution containing TiO_2

NPs before irradiation, and temperatures ranging from 15 to 40 °C.

In addition, the reactive oxygen species (ROS) responsible for the photocatalytic degradation of IBU were identified by monitoring its degradation in the presence of TiO_2 NPs after the addition of small amounts of either *t*-BuOH or *p*-BQ, which scavenge for $OH^{\bullet}$ and $O_2^{\bullet -}$ radicals, respectively. The effect of additional H_2O_2 on the photocatalytic degradation of IBU was also assessed by adding a small amount of the oxidizing agent. Each photocatalytic experiment was performed in duplicate, and the average value was used for analysis.

2.6 Kinetic, diffusion, and thermodynamic analyses

The degradation kinetics and rate of IBU due to direct photolysis under 365-nm light irradiation were inspected based on the first-order reaction model:[28,29,35]

$$C_t = C_0\, e^{-k_p t} + C \quad (3)$$

Here, k_p (in min^{-1}) is the observed photolytic rate constant, C is the residual IBU concentration at prolonged irradiation time, and $C_0 - C$ is the extent of IBU degradation rate.

On the other hand, the photocatalytic degradation kinetics and rate of IBU were deduced by fitting the experimental data to the L–H kinetic model;[28,35,37,38]

$$dC/dt = k_{obs}{}^{K_L C}/(1 + K_L C) \quad (4)$$

where k_{obs} is the observed photocatalytic degradation rate constant, and K_L is the Langmuir adsorption isotherm constant.

Temperature-dependent photocatalytic degradation kinetics were analyzed using the Eyring and Arrhenius equations, given respectively as[29,39]

$$k_{obs} = (k_B T/h) e^{-\Delta G/RT} \quad (5)$$

$$k_{obs} = A\, e^{-E_a/RT} \quad (6)$$

where k_B is the Boltzmann constant, T is the temperature of the medium, h is the Planck constant, ΔG is the Gibbs free energy change, R is the gas constant, A is the Arrhenius pre-exponential factor, E_a is the activation energy for the photocatalytic degradation of IBU. By applying the standard Gibbs free energy relationship, $\Delta G = \Delta H - T\Delta S$, eqn (5) can be rewritten as

$$k_{obs} = (k_B T/h) e^{-\Delta H/RT + \Delta S/R} \quad (7)$$

where ΔH and ΔS represent the changes in enthalpy and entropy of the photocatalytic degradation of IBU, respectively. The thermodynamics parameters were determined from the linear plots of $\ln k_{obs}$ and $R \ln(hk_{obs}/k_B T)$ as functions of T^{-1}.

All curve-fitting analyses were carried out using Origin 6.0 software.

2.7 Identification of photocatalytic degradation products

The chemical structures and functional groups of the photocatalytic degradation products of IBU were identified using LC-MS and FTIR spectroscopic techniques. After 100 minutes of photocatalytic degradation, the TiO_2 photocatalysts were removed by centrifugation, and the solution containing the IBU degradation products was collected and dried in an oven at 40 °C. The resulting dried solid was divided into two portions, which were respectively used for LC-MS and FTIR analyses.[35]

LC-MS analysis was performed using a Nexera LC-40 XS Modular HPLC system (Shimadzu, Kyoto, Japan) with a 150 × 2.1 mm column. The mobile phase was 0.1% (v/v) acetic acid in water, with an injection volume of 20 μL and a flow rate of 0.2 mL min^{-1}.

Separation of the photocatalytic degradation products was achieved using a binary solvent gradient, increasing from 2% to 50% and then to 98% at 5 and 10 minutes, respectively. Electrospray ionization was applied in both negative and positive modes at a temperature of 400 °C. Nitrogen gas was utilized as both the drying and nebulizing gas at a flow rate of 5 L min^{-1}, with a drying temperature of 300 °C. Mass spectra were acquired over the m/z range of 50–2000 with a scan time of 0.1 s.[35]

FTIR analysis of the photocatalytic degradation products of IBU was performed using the KBr pellet method. The FTIR spectra were scanned in the range of 4000–400 cm^{-1} using a Spirit FTIR spectrometer (Shimadzu, Japan). The FTIR spectrum of IBU before photocatalysis was also measured for comparison. Based on the LC-MS and FTIR results, the chemical structures were constructed using ChemSketch, and were further confirmed by comparison with known compounds in the ChemSpider database.[35]

2.8 Antibacterial activities and toxicity tests

The antibacterial activity and toxicity assessment of photocatalytic degradation products of IBU have been adapted from Shahri *et al.*, with slight modifications.[40] Antibacterial activity was screened against both Gram-positive *Bacillus subtilis* (ATCC 6633) and Gram-negative *Escherichia coli* (ATCC 25922) using the agar well diffusion method. Bacterial cultures were prepared by incubating the strains in sterile nutrient broth at 37 °C overnight in an incubator. The cultures were then adjusted to a 0.5 McFarland standard based on absorbance at 625 nm, in the range of 0.08–0.13, corresponding to an approximate bacterial density of 1.5×10^8 CFU mL^{-1}.[41] A volume of 200 μL of the bacterial suspension was spread onto sterile Muller-Hinton agar plates and allowed to dry. After drying, four wells with a diameter of 5 mm were created using a cork borer. Two wells were filled with 40 μL of the solution containing the photocatalytic degradation products of IBU. The remaining two wells were respectively filled with ultrapure water as the negative control and streptomycin as the positive control. Streptomycin was selected as the positive control due to its well-known effectiveness against both Gram-positive and Gram-negative bacteria.[42] The plates were then incubated at 37 °C overnight, and the diameters of the inhibition zones were measured. The screening tests were repeated at least in duplicate, and inhibition zones were reported as the average values. For comparison, the antibacterial activity of 2 mg mL^{-1} IBU before photocatalysis was also evaluated.

The toxicity of the photocatalytic degradation products of IBU was assessed using a brine shrimp (*Artemia nauplii*) lethality bioassay in a 12-well plate.[40] Brine shrimp eggs were purchased from a local supplier and hatched at room temperature for 48 hours in artificial seawater prepared from water solution of commercial sea salt. Ten brine shrimps were transferred into each well, followed by the addition of 0.5 mL (200, 20, 2, 0.2 mg L^{-1}) of the solution of photocatalytic degradation products of IBU and 3.5 ml of artificial seawater, resulting in an approximate final concentration of 25, 2.5, 0.25, and 0.025 μg L^{-1} per well. The plates were then incubated at room temperature overnight, and the number of surviving brine shrimps were counted in the following day. Toxicity was expressed as the 50% lethal concentration (LC50), defined as the concentration at which 50% of the brine shrimp population per well lethally affected.

3. Results and discussion

3.1 Adsorption and direct photolysis of ibuprofen

Adsorption of IBU at various initial concentrations onto a certain dosage of TiO_2 photocatalyst in batch mode was revealed by the decrease in absorbance in the UV-vis absorption spectra, as shown in Fig. S2. Based on their absorbance and the molar extinction coefficient at 262.5 nm, the initial (C_0) and equilibrium (C_e) concentrations of IBU were determined, and the adsorption capacity (Q_e) of IBU on the photocatalyst surfaces was quantified. The plot of Q_e as a function of C_e is shown in Fig. 1(a).

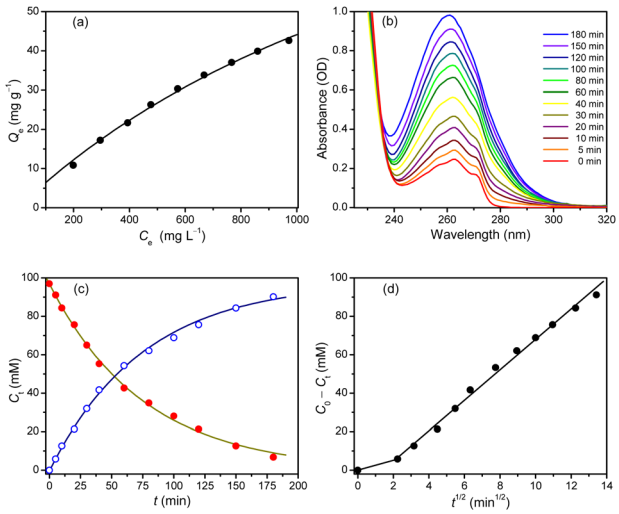

Fig. 1 (a) Adsorption isotherm data of IBU (●) on TiO_2 NPs fitted with the Langmuir isotherm model (▬); (b) UV-vis absorption spectra of 200 mg L^{-1} IBU in the presence of 2.5 mg TiO_2 NPs under UV-light irradiation at different irradiation times, as indicated; (c) concentrations of IBU (●) and its photocatalytic degradation products (○) fitted with the modified Langmuir–Hinshelwood model; and (d) plot of $C_0 - C_t$ *versus* $t^{1/2}$, revealing two linear segments with a breakpoint that indicates significant external mass-transfer resistance at early irradiation times.

The adsorption isotherm data of IBU on TiO_2 NPs simulated using the nonlinear equations of the Dubinin–Radushkevich, Elovich, Freundlich, Jovanović, Langmuir, and Temkin models are shown in Fig. S3. Since all these isotherm models have the same levels of parameters, a direct comparison of their R^2 and χ^2 values was used to assess the suitability and accuracy of each model in fitting the experimental data. Based on these criteria, as summarized in Table S1, the adsorption isotherm of IBU was best described by the Langmuir model, which exhibited the highest R^2 (0.997) and lowest χ^2 (0.475). The suitability of the Langmuir model also supports the application of the L–H kinetic model in analyzing the photocatalytic degradation process.

The best fit of the Langmuir isotherm model revealed the maximum adsorption capacity (Q_m) of 126 ± 4 mg g^{-1} (or equivalent to 0.612 ± 0.018 mmol g^{-1}) and a Langmuir isotherm constant (K_L) of 5.40 ± 0.7 ×10^{-4} L mg^{-1}. These findings suggest high immobilization and efficient adsorption of IBU on TiO_2 NPs, which is significantly higher than that reported on chitosan (24.21 mg g^{-1})[14] and slightly lower than that of activated carbon derived from sisal waste *via* chemical activation with K_2CO_3 (145.2 mg g^{-1}).[12] This behavior is due most likely to the strong affinity of the carboxylic acid group of IBU toward the oxygen atoms on the surfaces of TiO_2 NPs. This interpretation is further supported by the relatively low K_L value, which suggests that a high IBU concentration is required to reach adsorption–desorption equilibrium.

For direct photolysis, as shown in Fig. S4(A), IBU exhibits no changes in absorbance under 365 nm light irradiation, even after prolonged exposure times of up to 180 minutes. The fine-structured absorption spectrum, which arises from vibronic transitions, also remains unchanged. The results suggest that the chemical and conformational structure of IBU remains entirely intact, as this analgesic compound is not effectively excited by 365-nm light photons. In other words, IBU undergoes negligible degradation *via* direct photolysis. The addition of H_2O_2 also did not result in observable degradation of IBU by the photolysis, emphasizing that direct oxidation of IBU by H_2O_2 or by $OH^{\bullet}$ radicals generated through photodissociation of the oxidizing agent in solution is negligible. Such inefficient oxidation by UV/H_2O_2 treatment is not unexpected, as the photodissociation efficiency of H_2O_2 in solution under UV irradiation at wavelengths longer than 250 nm is very low.

Nevertheless, the degradation kinetics and rate of IBU by the direct photolysis were analyzed. Referring to the first-order kinetic model, given in eqn (2), the relative concentration (C_t/C_0) of IBU was plotted as a function of irradiation time, t, and was simulated using a single-exponential decay, as shown in Fig. S4(B). The best fit yielded the k_p value of 3.27 × 10^{-3} min^{-1} with degradation efficiency being less than 2% after 180 minutes of irradiation. Under the same experimental conditions, the degradation kinetics and rate of IBU are significantly lower than those reported for rifampicin and cephalexin antibiotics, where the k_p values are 1.67 × 10^{-2} min^{-1} [28] and 1.85 × 10^{-2} min^{-1} [29] with efficiencies being about 7.2% and 3.0%, respectively. These results further confirm that IBU is

considerably more resistant to direct photolytic degradation than these antibiotics.

3.2 Photocatalytic degradation of ibuprofen

The photocatalytic degradation behavior of IBU was revealed by changes in its absorption spectrum, as shown in Fig. 1(b). Interestingly, the fine-structured absorption spectrum progressively overlapped with each other as the irradiation time increased, resulting in a broad spectral profile accompanied by a gradual increase in absorbance. This behavior is in contrast with the typical photocatalytic degradation of organic compounds, which is generally characterized by a continuous decrease in absorbance due to mineralization into small volatile compounds such as carbon dioxide, ammonium hydroxide, and water, which are not detected by UV-vis spectroscopic measurements. Therefore, it is reasonable to consider that the spectra observed in Fig. 1(b) are actually an overlap between the absorption spectrum of IBU and those of its photocatalytic degradation products, which exhibit spectral features similar to those of the photocatalytic degradation product, 1-(4-isobutylphenyl)ethanol, reported by Cory *et al.*[23] Since the spectrum was obtained after more than 200 h of UV-A light irradiation (0.8–1.1 mW cm^{-2}), it is reasonable to assume that it was originated uniquely from the degradation products generated from IBU during photocatalytic degradation. Based on this assumption, the absorption spectra shown in Fig. 1(b) were deconvoluted using a linear combination of the absorption spectra of IBU and the photocatalytic product as references, employing non-negative least square optimization in Mathematica 10 software. The representative results are presented in Fig. S5. Using this spectral deconvolution approach, the concentrations of IBU and its photocatalytic products were plotted as a function of irradiation time, t, as shown in Fig. 1(c).

The kinetics of photocatalytic degradation of IBU was subsequently analyzed using the L–H model (eqn (4)). Given that the K_L value for IBU adsorption on TiO_2 NPs is on the order of 10^{-4} L mg^{-1} and C_0 of IBU is 200 mg L^{-1}, the condition $K_L C \ll 1$ is satisfied. Under this condition, integration of eqn (4) analytically lead to the simplified L–H kinetic model;[37,38]

$$C_t = C_0 e^{-k_{obs} t} + C_{ec} \quad (8)$$

which is analogous to the first-order kinetic model given in eqn (3). Here, C_{ec} represents the equilibrium concentration of IBU at prolonged irradiation times, and the term $C_0 - C_{ec}$ corresponds to the extent of photocatalytic degradation.

From the best global fitting of eqn (8) to the kinetic data for IBU degradation, as shown in Fig. 1(c), the k_{obs} value was estimated to be $1.31 \pm 0.02 \times 10^{-2}$ min^{-1}. This value is slightly lower than those for the overall photocatalytic degradation of cephalexin (2.30×10^{-2} min^{-1}) and rifampicin (1.63×10^{-2} min^{-1}) on TiO_2 NPs under the same experimental conditions.[28,29] Given that the typical coverage coefficients of these pharmaceutical compounds on TiO_2 NPs are comparable, within the range of 1.5×10^{-3} to 1.8×10^{-3} L mg^{-1}, the photoreaction coefficient of IBU, which is linearly related to the rate constant of the photocatalytic degradation, was lower than those of cephalexin and rifampicin. This indicates that IBU is significantly more resistant to photocatalytic degradation than these antibiotics. A plausible explanation for the lower photoreaction coefficient of IBU is the limited reactive radicals that are capable to oxidize this analgesic compound.

As shown in Fig. 1(c), the photocatalytic degradation rate is essentially high. The degradation efficiency for 200 mg L^{-1} IBU using 2.5 mg TiO_2 NPs was as high as 95%. In comparison, under the same experimental conditions, the photocatalytic degradation efficiency of 75 mg L^{-1} cephalexin using 2.5 mg TiO_2 NPs was about 68%, while that of 50 mg L^{-1} rifampicin using 1.0 g TiO_2 NPs was 87%. These findings emphasize that the intermediate species and degradation products resulting during the photocatalytic oxidation reaction of IBU by ROS generated on the surfaces of TiO_2 NPs may rapidly escape from the solvent cage in the close vicinity of the photocatalyst surfaces.[43] In this context, the relatively simple aromatic structure of IBU, as well as its photocatalytic degradation intermediates and products, are less steric hindrance than those of cephalexin and rifampicin. A similar interpretation has been pointed out in the higher, faster, and more efficient photocatalytic degradation rate of methylene blue, which is relatively more planar and less sterically hindered compared to rhodamine B and auramine O.[38]

It is important to emphasize that both the photocatalytic degradation of IBU and the formation of its degradation products proceed with the same rate constant while conserving the total concentration. This observation suggests that photocatalytic degradation largely conserves the aromatic ring of IBU, converting it into 1-(4-isobutylphenyl) derivatives, rather than being further mineralized into carbon dioxide and water. This behavior highlights the stable formation of recalcitrant degradation products which can repel further rapid oxidation by radical attacks. This interpretation is supported by the steady absorbance of UV-vis absorption spectrum of IBU upon photocatalysis at prolonged irradiation times.[23] This behavior is in contrast to the more complex degradation pathways of IBU associated with persulfate- and hydroxylamine-based oxidation systems.[44,45]

The kinetics of photocatalytic degradation of IBU are generally governed by the diffusion and immobilization of the pharmaceutical compound on the photocatalyst surfaces. To verify this viewpoint, the kinetic data were analyzed using the Weber–Morris intraparticle diffusion model;[46]

$$C_0 - C_t = k_i t^{1/2} + C_1 \quad (9)$$

where, k_i and C_1 denote the intraparticle diffusion rate constant and the boundary layer thickness, respectively. In fact, the plot of $C_0 - C_t$ *versus* $t^{1/2}$ revealed two linear segments with a breakpoint at around $t^{1/2} = 2.15$ $min^{1/2}$, as shown in Fig. 1(d). During the initial irradiation period, the k_i value was 2.43 mM $min^{-1/2}$ with a negligible boundary layer thickness, followed by a faster diffusion stage with the k_i value of 7.92 mM $min^{-1/2}$ at longer irradiation times. This Weber–Morris plot suggests that IBU diffusion is primarily governed by mass transfer from the bulk solution to the photocatalyst surfaces, with external mass

transfer resistance being significant during the first 4.62 minutes of irradiation.

The effect of photocatalyst dosage on the photocatalytic degradation of IBU was investigated by monitoring the absorption spectra after 100 minutes of irradiation in the presence of different TiO_2 dosages ranging from 2.5 to 15 mg, as shown in Fig. S6. The absorbance increased nonlinearly with increasing catalyst dosage. This trend suggests that the formation of photocatalytic degradation products of IBU increased with TiO_2 dosage, and tends to saturate at higher photocatalyst dosages. Accordingly, the degradation efficiency of IBU is nonlinearly enhanced before reaching saturation. The spectra were then carefully deconvoluted, and the concentrations of IBU and its photocatalytic degradation products are presented in Fig. 2(a). It is clearly observed that, upon photocatalytic treatment with 15 mg TiO_2 NPs, the initial IBU concentration of 200 mg L^{-1} decreased to nearly zero, with the compound being almost completely converted into its photocatalytic degradation products.

It is worth noting that the photocatalytic degradation behavior of pharmaceutical compounds is closely associated with the ROS generated during photocatalysis.[22] In particular, with the standard reduction potential of conduction band typically around −0.28 V *vs.* NHE and that of valence band around +3.2 V *vs.* NHE, the photogenerated electron–hole pair of anatase TiO_2 NPs that migrated to the photocatalyst surfaces readily react with solvated oxygen and water molecules to produce $O_2^{\bullet-}$ and $OH^{\bullet}$ radicals, respectively. To identify the responsible reactive species for the degradation process, photocatalytic degradation of IBU was investigated in the presence of radical scavengers. Fig. S7 shows the absorption spectra of IBU solutions before and after photocatalysis on TiO_2 NPs in the presence of various concentrations of *t*-BuOH and *p*-BQ, which act as scavengers for $OH^{\bullet}$ and $O_2^{\bullet-}$ radicals, respectively, generated on the photocatalyst surfaces upon light excitation. The absorption spectra increasingly resembled that of pristine IBU upon the addition of higher concentrations of *t*-BuOH, whereas the spectra remained nearly unchanged upon the addition of *p*-BQ. Spectral deconvolution further confirmed that, as shown respectively in Fig. 2(b) and (c), the photocatalytic degradation of IBU was significantly suppressed in the presence of *t*-BuOH, while it was not noticeably affected by *p*-BQ. This scavengers study unambiguously indicates that the photocatalytic degradation of IBU on TiO_2 NPs is solely due to oxidation reaction by $OH^{\bullet}$ radicals. Since photocatalysts may also generate reactive singlet oxygen molecule ($^1O_2$), the photocatalytic degradation of IBU *via* singlet oxygen was further examined using rose bengal as photosensitizer under visible light irradiation. Since no changes in the absorption spectra were observed, even after prolonged irradiation times of up to 180 minutes, it can be concluded that IBU was hardly oxidized by singlet oxygen.

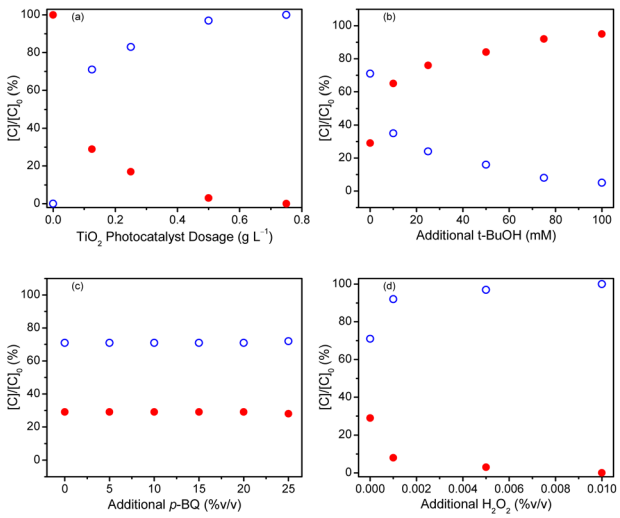

Fig. 2 Concentrations of IBU (●) and its photocatalytic degradation products (○) after 100 minutes of irradiation, showing the effects of (a) photocatalyst dosage, (b) addition of *t*-BuOH, (c) addition of *p*-BQ, and (d) addition of H_2O_2.

It is noteworthy that the photocatalytic degradation of various classes of antibiotics, including rifampicin and cephalexin, on TiO_2 or $SrTiO_3$ NPs can be achieved by both the generated $OH^{\bullet}$ and $O_2^{\bullet-}$ radicals (see Table S2). The dominant role of $OH^{\bullet}$ radicals in the degradation of IBU can be rationalized from a redox (reduction–oxidation) perspective. Given the standard reduction potentials of ROS, including $OH^{\bullet}$, $SO_4^{\bullet-}$, $O_2^{\bullet-}$, and $^1O_2$ which are approximately +2.8 V, +2.6 V, +0.91 V, and +1.24 V *vs.* NHE, respectively, the overall results suggest that that the oxidation potential of IBU lies below +2.6 V but above +1.24 V *vs.* NHE. Consequently, the relatively high oxidation resistance of IBU necessitates ROS with high reduction potentials for its effective degradation. The high oxidation resistance of IBU is also supported by previous observations of IBU degradation on $BaTiO_3$ NPs *via* piezoelectric catalytic activation of persulfate, which continuously generates $SO_4^{\bullet-}$ and $OH^{\bullet}$ radicals. In this case, the comparable high standard reduction potentials of $SO_4^{\bullet-}$ and $OH^{\bullet}$ radicals were the reason for their contributions (approximately 53% and 44%, respectively) to the overall degradation of IBU.[47] It is also interesting to note that, with the standard potential of the valence band of anatase TiO_2 NPs being about +3.2 V *vs.* NHE, direct oxidation of IBU by photogenerated holes (h^+) *via* electron abstraction is thermodynamically feasible. However, the contribution of hole direct oxidation is likely minor under these conditions, as this process requires the immobilization of IBU on the photocatalyst surfaces. In contrast, the oxidation of surface-adsorbed water molecules by holes to generate $OH^{\bullet}$ radicals is more competitive and thus dominates the photocatalytic degradation of IBU.

Considering the critical role of $OH^{\bullet}$ radicals in the photocatalytic degradation of IBU on TiO_2 NPs, further evidence can be obtained by the addition of H_2O_2, which accelerates the generation of $OH^{\bullet}$ radicals. The effect of varying amounts of added H_2O_2 on the photocatalytic degradation of an initial IBU concentration of 200 mg L^{-1} (0.97 mM) is reflected by the absorption spectra shown in Fig. S8. Based on spectral deconvolution, the extent of IBU degradation increased nonlinearly from 0.69 mM in the absence of H_2O_2 to 0.88, 0.93, and 0.96 mM in the presence of additional 0.001%, 0.005%, and 0.010% v/v

H_2O_2 in 20 mL solution of IBU, as shown in Fig. 2(d). Notably, the initial 0.97 mM IBU was almost completely degraded and converted into degradation products after 100 minutes of photocatalysis using 2.5 mg TiO_2 NPs in the presence of 0.010% v/v H_2O_2. The results demonstrate enhanced photocatalytic degradation of IBU upon the addition of a small amount of H_2O_2, which may arise from either the UV light-induced photodissociation of H_2O_2 to generate additional $OH^{\bullet}$ radicals in the solution,[48] or scavenging of photogenerated electrons on the photocatalyst surfaces.[49] However, considering that the diffusion coefficient of IBU is 5×10^{-10} m^2 s^{-1}, and the lifetime of $OH^{\bullet}$ is about 20 ns, during which IBU diffuses only within 10 nm^2, the oxidation reaction of IBU in the solution should be less pronounced. Therefore, the enhancement effect of H_2O_2 on the photocatalytic degradation of IBU is more likely attributable to photogenerated electron scavenging, which suppress electron–hole recombination and accelerates $OH^{\bullet}$ radical formation on the photocatalyst surfaces.[50] The increased degradation rate of IBU on TiO_2 NPs in the presence of H_2O_2 provides further evidence for the crucial role of $OH^{\bullet}$ radicals in the photocatalytic process.

It is well known that IBU exhibits acidic characteristic with a pKa of 4.91, which is related to its pharmacological action in inhibiting enzymes responsible for inflammation, pain, and fever.[51] IBU undergoes a transition from its neutral to an anionic form at pH 4.91 due to protonation and deprotonation of the carboxylic group. Therefore, the pH of the medium is an important factor determining the photocatalytic degradation of IBU. The ambient pH of IBU solution was fairly neutral, while acidic and alkaline conditions were adjusted by adding a few drops of 0.1 M HCl or 0.1 M NaOH, respectively. As shown in Fig. S9(a), before photocatalysis, IBU solutions in the pH range of 4–10 exhibited similar absorption spectral features, although the absorbance increased with pH of the medium. This observation suggests that the conformational structure of IBU remains intact across this pH range, while the oscillator strength of IBU anion increases due to higher electron delocalization. Nevertheless, changes in the ionic state strongly affect the immobilization, electrostatic interactions, and photocatalytic degradation rate of IBU on the surfaces of TiO_2 NPs.[52] Therefore, pH of medium is a crucial parameter governing the photocatalytic degradation behavior of IBU.

The absorption spectra of IBU after photocatalysis at different pH values are shown in Fig. S9(b), highlighting that the residual absorbance of IBU after photocatalysis depends strongly on the pH of the medium. Since no significant changes in the spectral feature were observed, it is reasonable to conclude that IBU degradation proceeds *via* similar pathways across the investigated pH range, while the increase in absorbance reflects a lower photocatalytic degradation rate of IBU. Spectral deconvolution confirmed that the photocatalytic degradation rate of IBU decreased sharply from pH 4 to 5, followed by a nearly linear decrease with increasing pH, as shown in Fig. 3(a). The results straightforwardly indicate that the photoreaction coefficient of protonated IBU is higher than that of its deprotonated form, and that photocatalytic degradation is more efficient under acidic conditions than under alkaline

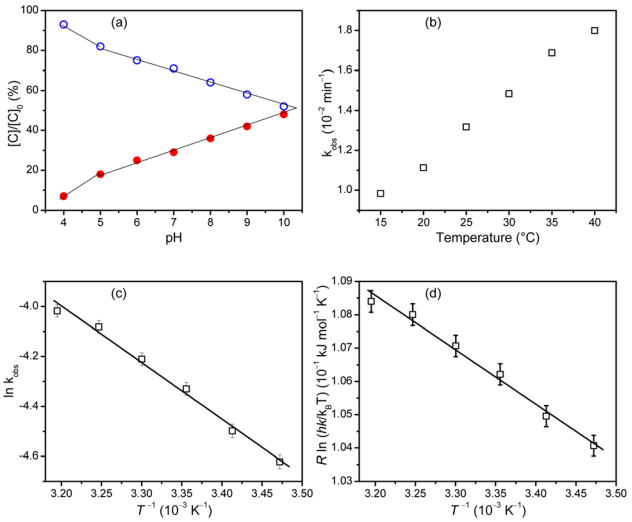

Fig. 3 (a) Relative concentrations (C/C_0) of IBU (●) and its photocatalytic degradation products (○) after 100 minutes of irradiation at different pH values; (b) temperature dependence of the observed rate constant (k_{obs}); (c) linear plot of ln k_{obs} *versus* T^{-1}; and (d) linear plot of $R \ln(hk_{obs}/k_BT)$ *versus* T^{-1}.

conditions. This finding can be attributed to the point of zero charge of TiO_2 NPs (pH 6.1),[53] above which electrostatic interactions between anionic IBU and the negatively charged surface of the photocatalyst is inefficient, consequently diminishing the affinity of the negatively charged IBU toward the photocatalyst.

As the photocatalytic degradation kinetics of IBU are governed by its temperature-dependent diffusion from the solution to the surfaces of TiO_2 NPs, thermodynamic parameters were further elucidated based on the degradation behavior of IBU at different temperatures. Fig. S10 shows representative absorption spectra of IBU before and after photocatalysis, revealing higher absorbance changes at higher temperatures. This observation indicates that the photocatalytic degradation of IBU is accelerated at higher temperatures, most likely due to higher kinetic energy and mobility of IBU molecules in solution. These factors enhance the immobilization of the pharmaceutical compound onto the photocatalyst surfaces, thereby accelerating its photocatalytic degradation kinetics. The temperature-dependent k_{obs} value is presented in Fig. 3(b), and was used to estimate the thermodynamic parameters of the photocatalytic degradation of IBU using the Arrhenius and Eyring equations.

From the linear plot of ln k_{obs} *versus* T^{-1} shown in Fig. 3(c), the E_a value for the photocatalytic degradation of IBU was found to be 18.84 ± 0.56 kJ mol^{-1}, much higher than those reported for rifampicin (1.585 ± 0.079 kJ mol^{-1}) and cephalexin (3.949 ± 0.257 kJ mol^{-1}). The values of ΔH and ΔS were obtained from the slope and *y*-intercept of the linear plot of $R \ln(hk_{obs}/k_BT)$ *versus* T^{-1}, as shown in Fig. 3(d), to be 0.016 ± 0.001 kJ mol^{-1} and 0.161 ± 0.003 J mol^{-1} K^{-1}, respectively. Using these parameters, the ΔG values were calculated to be in the range from -0.030 to -0.034 kJ mol^{-1}. These thermodynamic parameters of photocatalytic degradation of IBU are

summarized in Table S3. The positive values of ΔH and ΔS indicate that the photocatalytic degradation of IBU is weakly endothermic and thermodynamically favorable, and is accompanied by an increase in disorder at the photocatalyst surfaces. The negative ΔG values further suggest that the photocatalytic degradation proceeds spontaneously on the surfaces of TiO_2 NPs under UV light irradiation.

3.3 Photocatalytic degradation pathways of ibuprofen

Full-scan LC-MS was employed to identify the photocatalytic degradation products of IBU. The results confirmed the presence of IBU ($m/z = 207$) the parent pharmaceutical compound along with three photocatalytic degradation products. Based on the LC-MS data, shown in Fig. S11, the degradation products generated through oxidation reaction of IBU were identified to be 1-(4-isobutylphenyl)ethanol (**P1**, $m/z = 179$), 4-isobutylbenzaldehyde (**P2**, $m/z = 163$), and 4-isobutyl-1-ethylbenzene (**P3**, $m/z = 161$). Accordingly, plausible photocatalytic degradation pathways, including intermediates and products, are proposed in Scheme 1. In the proposed pathway, the progressive degradation of IBU is triggered by $OH^{\bullet}$ radicals generated on the photocatalyst surfaces. The $OH^{\bullet}$ radicals attack the carboxylic acid or carboxylate groups of IBU, leading to abstraction of a hydrogen atom from the carboxylic acid of protonated IBU or abstraction of an electron from the carboxylate groups of anionic IBU, thereby forming a short-lived intermediate, **I1**. This intermediate subsequently undergoes decarboxylation to produce another transient intermediate, **I2**. On the photocatalyst surfaces, the intermediate **I2** reacts with $OH^{\bullet}$ radicals to form **P1** *via* hydroxylation or **P2** through demethylation, or alternatively react with photogenerated electrons followed by hydrogenation to form **P3**. Similar photocatalytic degradation products have been reported by Miranda *et al.*,[19] Jallouli *et al.*,[21] and Xue *et al.*[54]

The chemical structures of IBU degradation products, **P1–P3**, were confirmed by FTIR spectroscopy. The FTIR spectra of IBU before and after photocatalytic degradation, as shown in Fig. 4, exhibit significant differences. The FTIR spectrum of IBU

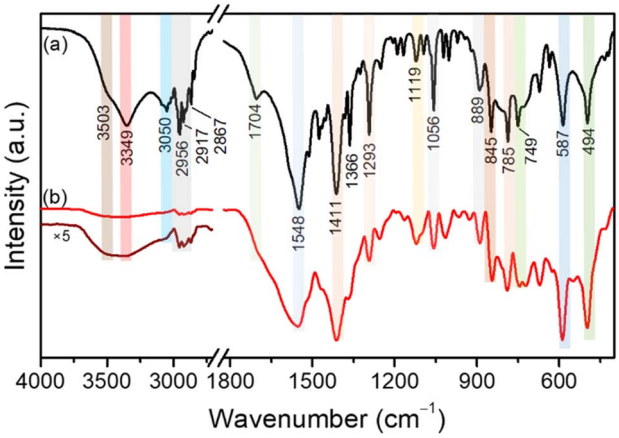

Fig. 4 FTIR spectra of IBU before (a) and after (b) photocatalytic degradation.

displays several intense bands at 3503 and 3349 cm^{-1}, which are assigned to the asymmetric and symmetric OH stretching vibrations of the carboxylic acid group. The bands observed at 2956, 2917, and 2867 cm^{-1} are due to the C–H bond in the benzene ring, methyl groups, and ethylene moiety, respectively. The band at 1704 cm^{-1} is due to the C=O stretching vibration. Bands at 1548, 1411, and 1119 cm^{-1} are attributed to the stretching vibrations of C=C in the benzene ring, C–C in aliphatic moieties, and C–O in the carboxylic group, respectively. The bands at 1293 and 1056 cm^{-1} are assigned to C–H vibrations, while those at 889, 845, 785, and 587 cm^{-1} arise from rocking and out-of-plane bending vibrations of C–H groups. Finally, the peaks at 749 and 494 cm^{-1} are attributed to skeletal vibrations.[55,56]

The FTIR spectra of IBU after degradation exhibit several bands that can be assigned to the presence of a small amount of residual IBU. Several prominent new bands are observed, particularly the two broad bands with peaks at 1548 and 1411 cm^{-1}, which confirm the C=C stretching vibrations in the benzene ring and the C–C stretching vibrations in the aliphatic moieties of **P1–P3**, respectively. The relatively unchanged vibrational bands at 587 and 494 cm^{-1} indicate that the out-of-plane C–H bending vibrations and skeletal vibrations remained unchanged. Therefore, FTIR spectral analysis confirms the chemical structures of the photocatalytic degradation products, **P1–P3**, which remain stable without further breakdown or complete mineralization, as proposed on the basis of LC-MS measurements. Nevertheless, further inorganic carbon analysis may be further needed to assess mineralization and minor products.

Based on the proposed photocatalytic degradation pathways, the observable overall rate constant, k_{obs}, depends on the relative magnitudes of $k + k'$ compared with $k_1 + k_2 + k_3$. The reaction of IBU with $OH^{\bullet}$ radicals, which is controlled by diffusion of the NSAID to the photocatalyst surfaces, is much slower than that of the following decarboxylation, hydroxylation, demethylation, and hydrogenation reactions. Therefore, it is reasonable to assume that k_{obs} value reflects the diffusion of IBU to the

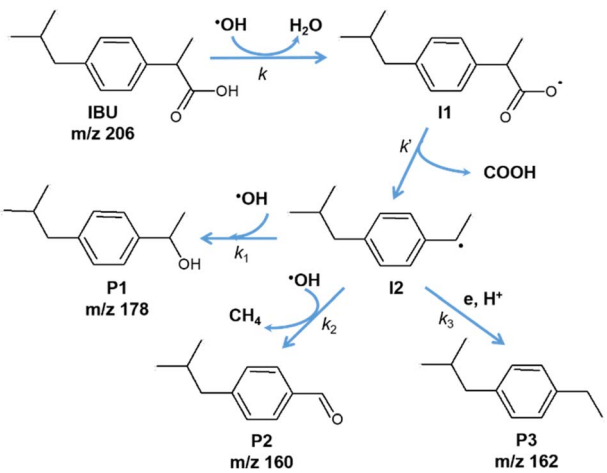

Scheme 1 Proposed photocatalytic degradation pathways of IBU.

photocatalyst surfaces and is proportional to the diffusion-limited reaction rate constant. Consequently, k_{obs} is related to the diffusion coefficient and the encounter distance of IBU and the photocatalyst surfaces, as described by the general Smoluchowski equation.[57]

3.4 Antibacterial activities and toxicity of ibuprofen and its degradation products

The antibacterial activities of IBU and its photocatalytic degradation products were screened against *E. coli* and *B. subtilis* using the well diffusion method. The results revealed no antibacterial activity, indicating that IBU and its persistent degradation products (**P1**, **P2**, and **P3**) are unable to inhibit peptidoglycan synthesis in the Gram-positive and Gram-negative bacterial cell walls. In contrast, both IBU and its photocatalytic degradation products exhibited toxicity against *A. salina* shrimp larvae.

Based on triplicate experiments conducted at concentrations of 200, 20, 2, and 2 mg L^{-1}, as summarized in Table 1, a total of 120 *A. salina* shrimp larvae were tested, and the average larval mortalities were in the range from 0 to 50%. Larval mortality increased nonlinearly with increasing IBU concentration, with the lethality concentration (LC50) approximately 175 mg L^{-1}, confirming that IBU exhibits moderate toxicity. After photocatalytic treatment, the larval mortality decreased significantly with increasing irradiation time, suggesting that the photocatalytic degradation products of IBU possess higher LC50 values. For example, the LC50 of IBU after 100 minutes of irradiation exceeded 1000 mg L^{-1}, strongly suggesting that the degradation products (**P1–P3**) may be non-toxic to *A. salina* shrimp under laboratory conditions. These results may indicate that the persistent photocatalytic degradation products of IBU are unlikely to pose significant toxicity risks to microorganisms in the environment. However, isolation of individual IBU degradation products and comprehensive toxicity evaluations, including animal testing, dose–response assessments, and other chemical risk analyses should be conducted in further detail to provide a clearer understanding of their toxicological effects and to more accurately determine the environmental safety of the resulting persistent degradation products.

Table 1 Average mortality of brine shrimp larvae in the presence of IBU before and after photocatalytic degradation at various irradiation times

	Concentration (mg L^{-1})	Irradiation time [min]	Mortality (%)
IBU	200	0	50
	20		17
	2		10
	0.2		0
	200	10	27
	20		10
	2		7
	0.2		0
	200	50	20
	20		7
	2		3
	0.2		0
	200	100	10
	20		3
	2		0
	0.2		0

4. Conclusions

The photocatalytic degradation of ibuprofen (IBU), a nonsteroidal anti-inflammatory drug (NSAID) widely utilized as an analgesic, antipyretic, and anti-inflammatory agent, was comprehensively investigated using anatase titania nanoparticles (TiO_2 NPs) as photocatalysts activated by 365-nm light irradiation. The Langmuir isotherm model indicated a high affinity of TiO_2 NPs toward IBU, with a maximum adsorption capacity of 126 $\pm$ 4 mg g^{-1}. While no photo-induced decomposition of IBU was observed upon direct photolysis, the NSAID compound underwent photocatalytic degradation. The photocatalytic degradation is driven solely by oxidation reaction of IBU by hydroxyl ($OH^{\bullet}$) radicals generated on the surfaces of TiO_2 NPs. This mechanism was further supported by the addition of a small amount of hydrogen peroxide which mediated $OH^{\bullet}$ formation and accelerated the photocatalytic degradation of IBU. The simplified Langmuir–Hinshelwood kinetic model revealed an observed degradation rate constant of 1.31 $\pm$ 0.02 $\times 10^{-2}$ min^{-1}. The limiting step of the degradation reaction was mass transfer of IBU to the photocatalyst surfaces. The degradation rate of protonated IBU was higher than that of its deprotonated form at pH values above the pK_a (4.91). Thermodynamic parameters were determined, where E_a is 18.84 $\pm$ 0.56 kJ mol^{-1}, ΔH is 0.016 $\pm$ 0.001 kJ mol^{-1}, ΔS is 0.161 $\pm$ 0.003 J mol^{-1} K^{-1}, and ΔG values in the range from -0.030 to -0.034 kJ mol^{-1}, suggesting the degradation was weakly endothermic, thermodynamically favorable, and spontaneous on the surfaces of TiO_2 NPs under UV light irradiation, followed by an increase in disorder at the photocatalyst surfaces. The chemical structures of the photocatalytic degradation of IBU were identified using LC-MS and FTIR analyses. The proposed degradation pathways involve $OH^{\bullet}$ radical attack on carboxylic acid group of IBU, followed by decarboxylation, hydroxylation, and demethylation to form intermediates and three stable products, namely 1-(4-isobutylphenyl)ethanol, 4-isobutylbenzaldehyde, and 4-isobutyl-1-ethylbenzene. Toxicity tests indicated that the photocatalytic degradation products of IBU are less toxic toward *A. salina* larvae, suggesting a reduced toxicity risk to microorganisms in the environment. Overall, this study provides valuable insights into the detailed kinetics, thermodynamics, and pathways of IBU degradation during photocatalytic treatment.

Author contributions

Conceptualization, A. U.; methodology, H. L. H. L., and A. U.; validation, A. U., H. T., and M. N.; formal analysis, A. U., H. L. H. L., S. N. A. A.; N. D. B. A. I.; N. A. A. M., N. N. R.; investigation, H. L. H. L., R. R. S., and S. N. A. A.; writing original draft, H. L. H. L., A. U.; writing review and editing, A. U.; visualization, A. U.;

supervision, H. T., M. N, and A. U. All authors have read and agreed to the published version of the manuscript. The authors received no financial support for the research, authorship, and/or publication of this article.

Conflicts of interest

There are no conflicts to declare.

Data availability

Supplementary information (SI): the characterization details of TiO_2 NPs used in this study and the absorption spectra of IBU detected before and after photocatalysis under various conditions. All data generated or analyzed during this study are included in this published article and its SI file. See DOI: https://doi.org/10.1039/d5ra10114j.

References

1 K. Placova, J. Halfar, K. Brozova and S. Heviankova, Issues of non-steroidal anti-inflammatory drugs in aquatic environments: A review study, *Eng. Proc.*, 2023, **57**, 13.
2 H. L. H. Lau, R. R. Sofian, S. N. A. Aewandy, N. D. B. A. Idris, N. A. A. Munir, N. N. Roslan, A. F. A. Majid, A. Usman and M. Nur, Pharmaceuticals as emerging contaminants in the environment: Impacts and remediation processes. in *Latest Research in Contaminants of Emerging Concern*, ed. D. Di Paola and C. Faggio, IntechOpen, London, United Kingdom, 2025, pp. 1–23.
3 M. Patel, R. Kumar, K. Kishor, T. Mlsna, C. U. Pittman Jr. and D. Mohan, Pharmaceuticals of emerging concern in aquatic systems: chemistry, occurrence, effects, and removal methods, *Chem. Rev.*, 2019, **119**, 3510–3673.
4 G. D. Alkimin, A. M. V. M. Soares, C. Barata and B. Nunes, Evaluation of ketoprofen toxicity in two freshwater species: Effects on biochemical, physiological and population endpoints, *Environ. Pollut.*, 2020, **265**, 114993.
5 A. Białk-Bielińska, Ł. Grabarczyk, E. Mulkiewicz, A. Puckowski, S. Stolte and P. Stepnowski, Mixture toxicity of six pharmaceuticals towards Aliivibrio fischeri, Daphnia magna, and Lemna minor, *Environ. Sci. Pollut. Res.*, 2022, **29**, 26977–26991.
6 P. Löffler, B. I. Escher, C. Baduel, M. P. Virta and F. Y. Lai, Antimicrobial transformation products in the aquatic environment: global occurrence, ecotoxicological risks, and potential of antibiotic resistance, *Environ. Sci. Technol.*, 2023, **57**, 9474–9494.
7 A. Marchlewicz, U. Guzik and D. Wojcieszyńska, Over-the-counter monocyclic non-steroidal anti-inflammatory drugs in environment–sources, risks, biodegradation, *Water, Air, Soil Pollut.*, 2015, **226**, 355.
8 A. Küster and N. Adler, Pharmaceuticals in the environment: scientific evidence of risks and its regulation, *Philos. Trans. R. Soc., B*, 2014, **369**, 20130587.
9 D. Sánchez, P. Velasco, N. Delgado, E. M. Jiménez-Bambague, J. C. Casas-Zapata, F. Machuca-Martínez and C. A. Madera-Parra, Impact of therapeutic pharmaceuticals on water bodies: diagnosis, ecological threat, and removal strategies, *Water Sci. Technol.*, 2025, **92**, 1187.
10 J. Jan-Roblero and J. A. Cruz-Maya, Ibuprofen: Toxicology and biodegradation of an emerging contaminant, *Molecules*, 2023, **28**, 2097.
11 C. André and F. Gagné, Cumulative effects of ibuprofen and air emersion in zebra mussels Dreissena polymorpha, *Environ. Toxicol. Pharmacol.*, 2017, **55**, 156–164.
12 A. S. Mestre, A. S. Bexiga, M. Proença, M. Andrade, M. L. Pinto, I. Matos, I. M. Fonseca and A. P. Carvalho, Activated carbons from sisal waste by chemical activation with K_2CO_3: Kinetics of paracetamol and ibuprofen removal from aqueous solution, *Bioresour. Technol.*, 2011, **102**, 8253–8260.
13 S. Mondal, K. Bobde, K. Aikat and G. Halder, Biosorptive uptake of ibuprofen by steam activated biochar derived from mung bean husk: equilibrium, kinetics, thermodynamics, modeling and eco-toxicological studies, *J. Environ. Manag.*, 2016, **182**, 581–594.
14 E. W. E. S. Shahrin, N. A. H. Narudin, N. N. M. Shahri, M. Nur, J.-W. Lim, M. R. Bilad, A. H. Mahadi, J. Hobley and A. Usman, A comparative study of adsorption behavior of rifampicin, streptomycin, and ibuprofen contaminants from aqueous solutions onto chitosan: Dynamic interactions, kinetics, diffusions, and mechanisms, *Emerging Contam.*, 2023, **9**, 100199.
15 S. C. Kollarahithlu and R. M. Balakrishnan, Adsorption of pharmaceuticals pollutants, ibuprofen, acetaminophen, and streptomycin from the aqueous phase using amine Functionalized superparamagnetic silica nanocomposite, *J. Clean. Prod.*, 2021, **294**, 126155.
16 M. Kwon, S. Kim, Y. Yoon, Y. Jung, T.-M. Hwang, J. Lee and J.-W. Kang, Comparative evaluation of ibuprofen removal by UV/H_2O_2 and UV/$S_2O_8^{2-}$ processes for wastewater treatment, *Chem. Eng. J.*, 2015, **269**, 379–390.
17 S. Zhou, L. Qiao, Y. Jia, S. K. Khanal, L. Sun and H. Lu, Micro-nano bubble ozonation for effective treatment of ibuprofen-laden wastewater and enhanced anaerobic digestion performance, *Water Res.*, 2025, **273**, 123006.
18 F. Méndez-Arriaga, S. Esplugas and J. Giménez, Degradation of the emerging contaminant ibuprofen in water by photo-Fenton, *Water Res.*, 2010, **44**, 589–595.
19 M. O. Miranda, W. E. C. Cavalcanti, F. F. Barbosa, J. A. de Sousa, F. I. da Silva, S. B. C. Pergher and T. P. Braga, Photocatalytic degradation of ibuprofen using titanium oxide: insights into the mechanism and preferential attack of radicals, *RSC Adv.*, 2021, **11**, 27720.
20 T. M. Khedra, S. M. El-Sheikha, A. A. Ismail and D. W. Bahnemann, Highly efficient solar light-assisted TiO_2 nanocrystalline for photodegradation of ibuprofen drug, *Opt. Mater.*, 2019, **88**, 117–127.
21 N. Jallouli, L. M. Pastrana-Martínez, A. R. Ribeiro, N. F. F. Moreira, J. L. Faria, O. Hentati, A. M. T. Silva and M. Ksibi, Heterogeneous photocatalytic degradation of ibuprofen in ultrapure water, municipal and

pharmaceutical industry wastewaters using a TiO2/UV-LED system, *Chem. Eng. J.*, 2018, **334**, 976–984.

22 N. N. Roslan, H. L. H. Lau, N. A. A. Suhaimi, N. N. M. Shahri, S. B. Verinda, M. Nur, J. W. Lim and A. Usman, Recent advances in advanced oxidation processes for degrading pharmaceuticals in wastewater–A review, *Catalysts*, 2024, **14**, 189.

23 C. Cory, W. Desantis and C. Z. Ulmer, Photodegradation of naproxen and ibuprofen and the formation of ecotoxic photoproducts in natural water systems, *IWA Specialty Conference on Natural Organic Matter*, Costa Mesa, CA, USA, 2011.

24 A. Fujishima and K. Honda, Electrochemical photolysis of water at a semiconductor electrode, *Nature*, 1972, **238**, 37–38.

25 V. Pandit, S. Arbuj, R. Hawaldar, P. Kshirsagar, U. Mulik, S. Gosavi, C.-J. Park and B. Kale, In situ preparation of a novel organo-inorganic 6,13-pentacenequinone–TiO2 coupled semiconductor nano-system: A new visible light active photocatalyst for hydrogen generation, *J. Mater. Chem. A*, 2015, **3**, 4338–4344.

26 S. L. N. Zulmajdi, N. I. I. Zamri, H. M. Yasin, E. Kusrini, J. Hobley and A. Usman, Comparative study on the adsorption, kinetics, and thermodynamics of the photocatalytic degradation of six different synthetic dyes on TiO_2 nanoparticles, *React. Kinet. Mech. Catal.*, 2020, **129**, 519–534.

27 N. A. A. Suhaimi, N. N. M. Shahri, J. H. Samat, E. Kusrini, J. W. Lim, J. Hobley and A. Usman, Domination of methylene blue over rhodamine B during simultaneous photocatalytic degradation by TiO_2 nanoparticles in an aqueous binary solution under UV irradiation, *React. Kinet. Mech. Catal.*, 2022, **135**, 511–527.

28 N. A. A. Suhaimi, M. K. H. Umar, H. L. H. Lau, N. N. Roslan, J. W. Lim, J. Hobley, M. Nur and A. Usman, An insight into the photocatalytic degradation of the antibiotic rifampicin by titanium dioxide nanoparticles in aqueous solution under UV light irradiation, *React. Kinet. Mech. Catal.*, 2024, **137**, 1105–1123.

29 N. N. Roslan, H. L. H. Lau, N. D. R. Jali, N. A. S. Yussof, M. Nur, H. Taha, E. Kusrini, S. Thongratkaew, K. Faungnawakij and A. Usman, Photocatalytic degradation of cephalexin antibiotic on TiO_2 nanoparticles: insights from kinetics, thermodynamics, liquid chromatography-mass spectrometry, degradation pathways, and antibacterial activities, *React. Kinet. Mech. Catal.*, 2025, **138**, 1175–1196.

30 L. Du, X. Liu, W. Huang and E. Wang, A study on the interaction between ibuprofen and bilayer lipid membrane, *Electrochim. Acta*, 2006, **51**, 5754–5760.

31 M. A. Asbollah, M. S. M. Sahid, K. M. Padmosoedarso, A. H. Mahadi, E. Kusrini, J. Hobley and A. Usman, Individual and competitive adsorption of negatively charged Acid Blue 25 and Acid Red 1 onto raw Indonesian kaolin clay, *Arabian J. Sci. Eng.*, 2022, **47**, 6617–6630.

32 A. F. A. Majid, R. Dewi, N. N. M. Shahri, E. W. E. S. Shahrin, E. Kusrini, N. Shamsuddin, J. W. Lim, S. Thongratkaew, K. Faungnawakij and A. Usman, Enhancing adsorption performance of alkali activated kaolinite in the removal of antibiotic rifampicin from aqueous solution, *Colloids Surf., A*, 2023, **676**, 132209.

33 A. F. A. Majid, N. A. N. H. Sofri, N. S. Mahdzidi, N. Shamsuri, S. Thongratkaew, K. Faungnawakij, M. Nur and A. Usman, Kaolin-based eco-friendly adsorbents for the removal of cephalexin antibiotic: Insights into kinetics, isotherm, mechanism, thermodynamics, and adsorbent regeneration, *J. Dispersion Sci. Technol.*, 2025, 2563809, DOI: 10.1080/01932691.

34 P. Sethi, S. Barman and S. Basu, Strategic tuning of GO ratios in CuBTC-GO nanocomposites for next-generation tetracycline adsorption: A deep dive into isotherms, kinetics, and thermodynamics, *Sep. Purif. Technol.*, 2025, **361**, 131311.

35 H. L. H. Lau, N. A. S. Yussof, N. N. Roslan, E. Kusrini, A. B. Prasetyo, H. Taha, S. Thongratkaew, K. Faungnawakij, M. Nur and A. Usman, Photocatalytic degradation of cephalexin and rifampicin antibiotics on cubic $SrTiO_3$ nanoparticles: kinetics, rate limiting steps, thermodynamics, degradation pathways, and bioactivities of photocatalytic degradation products, *React. Kinet. Mech. Catal.*, 2026, **139**, 689–718, DOI: 10.1007/s11144-025-02978-x.

36 P. Sethi, S. Barman and S. Basu, Eco-friendly tetracycline remediation using robust and highly reusable ZIF-67/g-C_3N_4 nanocomposites with coupled adsorption and photocatalytic pathways: A deep dive into isotherms, kinetics, thermodynamics, and degradation pathways, *ACS Sustainable Resour. Manage.*, 2026, **3**, 244–259.

37 P. Sun, J. Zhang, W. Liu, Q. Wang and W. Cao, Modification to L-H kinetics model and its application in the investigation on photodegradation of gaseous benzene by nitrogen-doped TiO_2, *Catalysts*, 2018, **8**, 326.

38 N. A. A. Suhaimi, N. N. Roslan, N. B. Amirul, H. L. H. Lau, A. A. Hasman, M. Nur, J. W. Lim and A. Usman, Unraveling the photocatalytic degradation kinetics and efficiency of methylene blue, rhodamine B, and auramine O in their ternary mixture: diffusion and conformational insights, *React. Kinet. Mech. Catal.*, 2024, **137**, 3441–3462.

39 Z. Ghasemi, H. Younesi and A. A. Zinatizadeh, Kinetics and thermodynamics of photocatalytic degradation of organic pollutants in petroleum refinery wastewater over nano-TiO2 supported on Fe-ZSM-5, *J. Taiwan Inst. Chem. Eng.*, 2016, **65**, 357–366.

40 N. N. M. Shahri, H. Taha, M. H. S. A. Hamid, E. Kusrini, J. W. Lim, J. Hobley and A. Usman, Antimicrobial activity of silver sulfide quantum dots functionalized with highly conjugated Schiff bases in a onestep synthesis, *RSC Adv.*, 2022, **12**, 3136.

41 P. P. Mahesh, J. Kolape, H. Sultana and G. Neelakanta, McFarland standards-based spectrophotometry method for calculating approximate multiplicity of infection for an obligate intracellular bacterium Anaplasma phagocytophilum, *Microorganisms*, 2025, **13**, 662.

42 A. Schatz, E. Bugie and S. A. Waksman, Streptomycin, a substance exhibiting antibiotic activity against gram-

positive and gram-negative bacteria. 1944, *Clin. Orthop. Relat. Res.*, 2005, **437**, 3–6.

43 C. Wang, H. Li, T. H. Bürgin and O. S. Wenger, Cage escape governs photoredox reaction rates and quantum yields, *Nat. Chem.*, 2024, **16**, 1151–1159.

44 W. D. Oh, Z. Dong and T. T. Lim, Generation of sulfate radical through heterogeneouscatalysis for organic contaminants removal: current development, challenges and prospects, *Appl. Catal., B*, 2016, **194**, 169–201.

45 R. Yin, L. Hu, D. Xia, J. Yang, C. He, Y. Liao, Q. Zhang and J. He, Hydroxylamine promoted Fe(III)/Fe(II) cycle on ilmenite surface to enhance persulfate catalytic activation and aqueous pharmaceutical ibuprofen degradation, *Catal. Today*, 2020, **358**, 294–302.

46 N. I. I. Zamri, S. L. N. Zulmajdi, N. Z. A. Daud, A. H. Mahadi, E. Kusrini and A. Usman, Insight into the adsorption kinetics, mechanism, and thermodynamics of methylene blue from aqueous solution onto pectin-alginate-titania composite microparticles, *SN Appl. Sci.*, 2022, **3**, 222.

47 F. Peng, R. Yin, Y. Liao, X. Xie, J. Sun, D. Xia and C. He, Kinetics and mechanisms of enhanced degradation of ibuprofen by piezo-catalytic activation of persulfate, *Chem. Eng. J.*, 2020, **392**, 123818.

48 M. Y. Kulikov, A. M. Feigin and O. Schrems, H_2O_2 photoproduction inside H_2O and H_2O:O_2 ices at 20–140 K, *Sci. Rep.*, 2019, **9**, 11375.

49 D. Saha, M. M. Desipio, T. J. Hoinkis, E. J. Smeltz, R. Thorpe, D. K. Hensley, S. G. Fischer-Drowos and J. Chen, Influence of hydrogen peroxide in enhancing photocatalytic activity of carbon nitride under visible light: An insight into reaction intermediates, *J. Environ. Chem. Eng.*, 2018, **6**, 4927–4936.

50 S. S. Shinde, C. H. Bhosale and K. Y. Rajpure, Hydroxyl radical's role in the remediation of wastewater, *J. Photochem. Photobiol., B*, 2012, **116**, 66–74.

51 M. S. Kaynak, M. Soyseven, B. Kaval, M. Çelebier, E. Aygeyik, S. Şahin and G. Arli, Exploring the correlation between ibuprofen solubility and permeability in intestinal disease conditions, *Acta Pharm. Sci.*, 2024, **62**, 593–609.

52 M. Zhang, P. A. Salvador and G. S. Rohrer, Influence of pH and surface orientation on the photochemical reactivity of SrTiO3, *ACS Appl. Mater. Interfaces*, 2020, **12**, 23617–23626.

53 M. Zeng, Influence of TiO_2 surface properties on water pollution treatment and photocatalytic activity, *Bull. Korean Chem. Soc.*, 2013, **34**, 953.

54 H. Xue, J. Li, G. Zhang, M. Li, B. Liu and C. Kang, Hydroxyl radical dominated ibuprofen degradation by UV/percarbonate process: Response surface methodology optimization, toxicity, and cost evaluation, *Chemosphere*, 2023, **329**, 138681.

55 M. Acharya, S. Mishra, R. N. Sahoo and S. Mallick, Infrared spectroscopy for analysis of co-processed ibuprofen and magnesium trisilicate at milling and freeze drying, *Acta Chim. Slov.*, 2017, **64**, 45–54.

56 E. C. Bogatinovska, K. Najkov, G. Petrushevski, N. Geskovski, V. Koleva and V. Stefov, Infrared and Raman spectra of racemic ibuprofen sodium dihydrate – Spectra-structure correlations, *Spectrochim. Acta, Part A*, 2025, **339**, 126190.

57 A. A. A. Suhaimi, C. P. Y. Kong, N. N. M. Shahri, M. Nur, J. Hobley and A. Usman, Dynamics of diffusion- and immobilization-limited photocatalytic degradation of dyes by metal oxide nanoparticles in binary or ternary solutions, *Catalysts*, 2022, **12**, 1254.